Available online at www.sciencedirect.com
SCIENCE DIRECT®
Applied Surface Science 223 (2004) 214–219
applied surface science
www.elsevier.com/locate/apsusc

Composition characterization of combinatorial materials by scanning X-ray fluorescence microscopy using microfocused synchrotron X-ray beam

Stefan Vogt[a], Yong S. Chu[a,*], Andrei Tkachuk[a], Petr Ilinski[a], Donald A. Walko[a], Frank Tsui[b]

[a]*Advanced Photon Source, Argonne National Laboratory, 9700 S. Cass Ave., Argonne, IL 60439-4856, USA*
[b]*Department Physics and Astronomy, University of North Carolina, Chapel Hill, NC 27599, USA*

Abstract

We describe a high-throughput scanning X-ray fluorescence (XRF) microscopy setup using a microfocused synchrotron X-ray beam, which is optimized for *in-parallel* X-ray characterization of composition and crystalline structure of combinatorial samples. We present X-ray fluorescence elemental maps of a full ternary $Co_xMn_yGe_{1-x-y}$ composition-spread thin film and discuss the quantitative analysis method used for obtaining the ternary composition.

PACS: 78.70.E; 61.10.Nz; 07.85.Qe; 68.37.Yz; 68.55.Jk

Keywords: CoMnGe; Composition-spread; X-ray fluorescence; X-ray diffraction; Synchrotron radiation instrumentation

1. Introduction

In recent years, the combinatorial approach has been providing a systematic high-throughput method for optimizing material functionalities of complex systems [1–3]. One of the combinatorial materials synthesis techniques is to produce composition-spread thin-films, in which the composition of two or more elements is varied continuously across the sample so that the physical property-functionality relation can be mapped out systematically as a function of composition [2]. Consequently, an accurate measurement of a sample's elemental composition is the most basic yet crucial step in combinatorial research.

X-ray fluorescence (XRF) is a two-step process [4]. Absorption of an incident X-ray photon ejects a core-level electron of a ground-state atom. The core electron-hole is then filled by an outer shell electron, resulting in emission of either a fluorescence X-ray photon or an Auger electron. Thus, the energy of the fluorescence X-ray photon is equal to the binding energy difference between the two electronic levels and the number of emitted photons is proportional to the number of excited atoms. Consequently, the measurement of an XRF spectrum quantifies the amount of specific elements in a sample. Since X-rays have much larger penetration depth into matter than charged particles (>1 μm for most solids at photon energies larger than 5 keV), an XRF measurement probes the

* Corresponding author. Tel.: +1-630-252-0150; fax: +1-630-252-0161.
E-mail address: ychu@aps.anl.gov (Y.S. Chu).

0169-4332/$ – see front matter © 2003 Elsevier B.V. All rights reserved.
doi:10.1016/S0169-4332(03)00895-X

bulk composition without the requirement of a vacuum environment. Moreover, the minimum detection level of X-ray probes is typically 10–1000 times better than that of charged-particle probes [5].

With synchrotron-based focusing instrumentation such as X-ray zone plates [6] and Kirkpatrick–Baez (KB) X-ray mirrors [7], scanning X-ray fluorescence microscopy has been extensively used for probing the elemental distribution within specimens with a high spatial resolution (a few microns to submicron) and low minimum detection level (a few parts per million) [8]. In characterizing combinatorial materials, we integrate both scanning XRF and X-ray diffraction (XRD) techniques in a single experimental setup so that elemental composition and crystalline structure can be mapped out in parallel. The integration of both techniques is possible because the XRF signal is insensitive to small changes in sample orientation required for the XRD measurement. This integrated approach for composition-spread samples is crucial not only for obtaining high-throughput compositional and structural characterization but also for completely eliminating possible systematical errors associated with correlating two separate measurements under different experimental settings. In this paper, we describe the synchrotron instrumentation for the scanning XRF/XRD and discuss quantitative XRF analysis of a ternary $Co_xMn_yGe_{1-x-y}$ composition-spread sample.

2. Experiment

The ternary sample of $Co_xMn_yGe_{1-x-y}$ was grown on a Ge(1 1 1) substrate using an advanced combinatorial MBE system [3]. A combination of computer-controlled sample rotation, masking, and source shutters was used for the combinatorial synthesis. A linear gradient thickness profile (wedge) for each of the precursors, i.e. Co, Mn, and Ge, was produced during deposition by moving a precision shadow mask across the substrate.

The 'height' of each wedge was about a monolayer. The precursors were deposited sequentially to form a trilayer, and the trilayers were repeated to produce a thick film. Co and Ge were evaporated from e-beam hearths, and Mn was from an effusion cell. The sample was grown at 250 °C and annealed at 450 °C. The sample was diamond shaped and about 1 cm^2 with a nominal film thickness of 600 Å.

X-ray characterization of the sample was carried out at an undulator beamline 7-ID (MHATT-CAT) of the Advanced Photon Source (APS) at Argonne National Laboratory. A schematic view of the experiment is shown in Fig. 1. X-rays produced by an APS type A undulator (3.3-cm periodicity) are monochromatized to 10 keV with a 1.4 eV FWHM bandwidth using a cryogenically cooled double-crystal Si(1 1 1) monochromator. A pair of KB mirrors, positioned 500 mm from the sample and 50 m from the source, were employed to focus the beam to a spot size of 5 μm (horizontal FWHM) × 12 μm (vertical FWHM) on the sample with an estimated flux density of 8×10^{11} photons/μm^2.

The ternary $Co_xMn_yGe_{1-x-y}$ composition-spread sample was mounted on a Newport six-circle kappa diffractometer for the parallel measurements of XRF and XRD. During the experiment, the sample was kept in an inert N_2 environment using a thin plastic bag, in order to avoid possible sample oxidation from ozone created by the intense X-ray beam. XRF spectra were collected using a compact Peltier-cooled Si drift diode energy-dispersive X-ray detector (50 mm^2 active area) [9]. In order to minimize the dead time, the detector

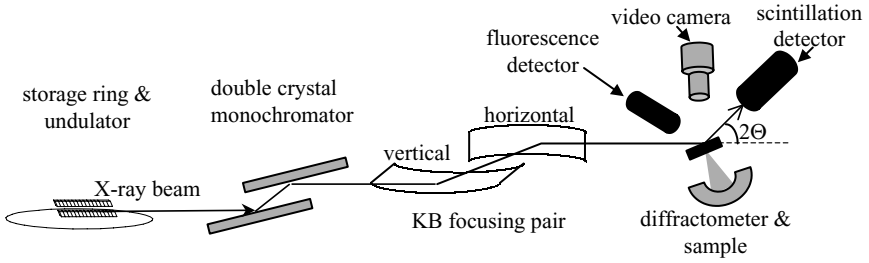

Fig. 1. Schematic view of the experimental setup.

signal was amplified with a shaping time of 0.12 μs, resulting in a modest energy resolution of 290 eV at 6 keV. Incident X-ray energy of 10 keV was chosen to avoid a large Ge fluorescence background from substrate Ge atoms. Consequently, only the Mn and Co concentrations are obtained from the XRF measurement. The scanning XRF measurements were carried out by performing two-dimensional raster scans of the sample through the focal spot of the beam using a sampling interval of 100 μm with a dwell time of 1 s per pixel.

3. Results and discussion

At each sampling point on the specimen, a full XRF spectrum was acquired to produce a three-dimensional (x, s, and energy) dataset. In Fig. 2, spectra averaged over three different regions on the sample are shown, together with an overview image displaying these spatial regions. These spectra exhibit several different peaks, corresponding to the specific energies of the X-ray photons measured by the detector. The intensities of some peaks do not depend on the sample position, because these do not correspond to features of the composition-spread thin film. For example, the elastic and Compton signals are due to scattering from the entire sample (film and substrate) and air. Consequently, the intensities of these peaks reveal the physical boundary of the sample, as shown in the inset of Fig. 2. The Ar Kα peak arises from argon atoms present in the air in front of the sample. XRF signals from other gases (nitrogen, oxygen, etc.) were not observed, because their fluorescence energies are below the detection limit of the experimental setup. The most dominant features of the composition-spread are the Kα (X-ray emission due to the electronic transition from L- to K-shell) and Kβ (M- to K-shell) emission lines of Co and Mn. Fluorescence lines of Ge are absent in the spectrum, because the incident beam energy of 10 keV is below the Ge K absorption-edge. The two minor peaks centered at 4.16 and 5.19 keV are Mn and Co escape peaks which originate from the escape of Si Kα fluorescence photon from the detector. The zinc signal in the spectrum is due to a trace amount of unexpected surface contamination.

In order to represent the two-dimensional composition distribution of the sample, we integrated over spectral regions of interest (ROI) corresponding to Mn Kα (from 5.778 to 6.018 keV) and Co Kα (from 6.810

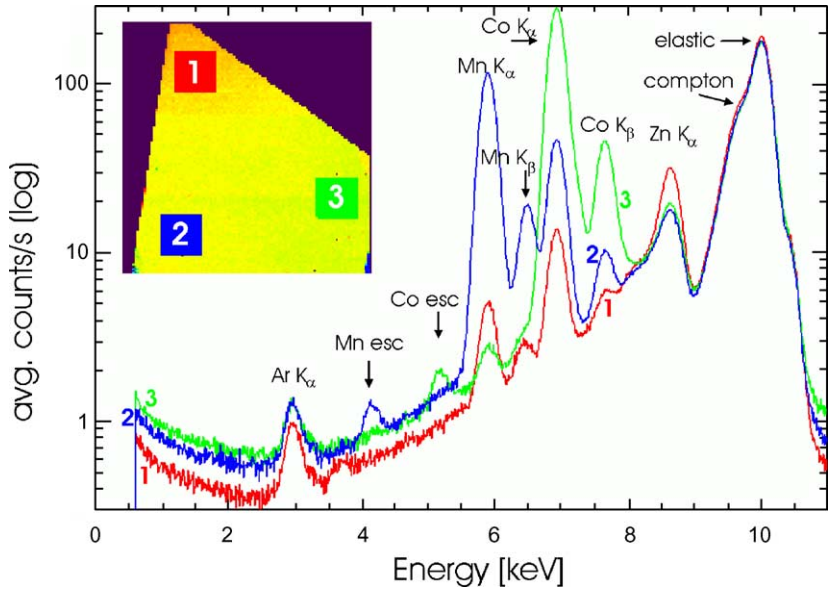

Fig. 2. Three X-ray fluorescence spectra, averaged over different regions in the sample, are shown in red, blue and green. The locations of the three regions are indicated in the total scattering (sum of elastic and Compton) intensity image of the sample shown in the inset. Co esc and Mn esc corresponds to Co and Mn escape peaks (see text).

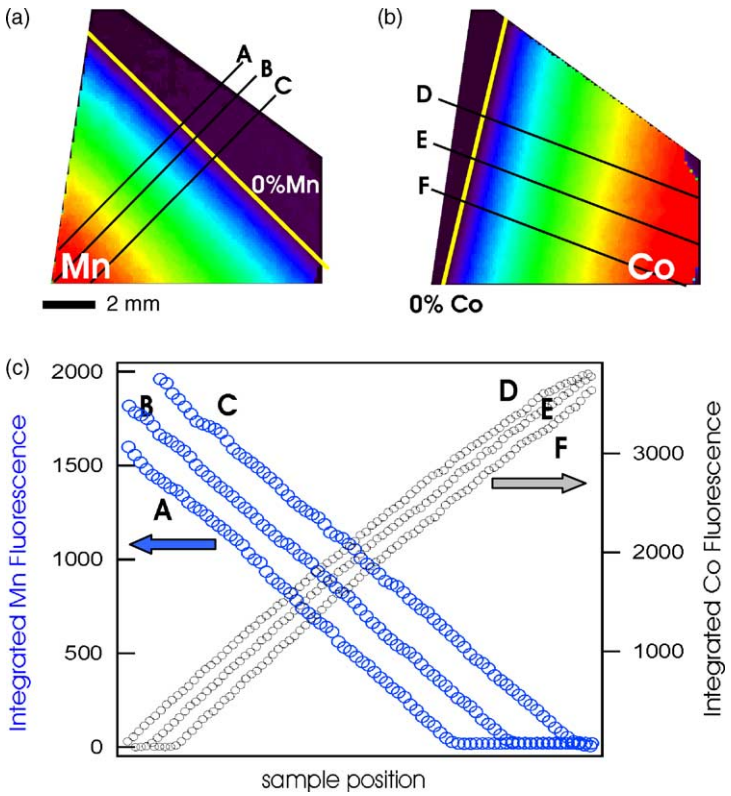

Fig. 3. Elemental distribution maps of (a) Mn and (b) Co. The intensity decreases from red to blue. The background-level intensity is indicated in black. The yellow line in each map marks the 0% concentration boundary. (c) One-dimensional intensity line profiles, extracted from the elemental maps. The locations of the profiles are shown in (a) and (b).

to 7.050 keV). The resulting Mn and Co elemental maps are shown in Fig. 3a and b. The yellow lines indicate the 0% composition boundaries. Both elemental maps exhibit homogeneous one-dimensional composition gradients along their respective directions, without any microscopic phase separation. The line profiles taken at various locations in the elemental maps exhibit excellent linearity, as shown in Fig. 3c.

These *raw* elemental maps are useful in characterizing the quality of the composition-spread growth for the individual elements. However, obtaining Mn/Co composition ratio from the measured Mn and Co XRF intensities requires several corrections listed in Table 1.

The differences in the absorption cross section and X-ray fluorescence yield between the two elements are intrinsic, solely due to differences in their interaction with the incident X-rays. The other extrinsic corrections are due to the fact that Mn Kα (5.899 keV) and Co Kα (6.930 keV) X-rays experience differential attenuation through the various materials along the path to the energy-dispersive detector. Consequently, we divided the measured Mn fluorescence intensity by

Table 1
Correction factors for obtaining composition ratio Mn/Co from the measured Mn Kα and Co Kα XRF intensities

Correction description	Correction factor (Mn/Co)
Absorption cross-section at 10 keV	0.837
X-ray fluorescence yield	0.855
Be window transmission (50 μm thickness)	0.991
Si dead layer transmission (0.3 μm thickness)	0.996
Polypropylene foil transmission (300 μm thickness)	0.901
Transmission through air (∼9 cm) and N_2 (∼3 cm)	0.885
Cumulative correction factor	0.563

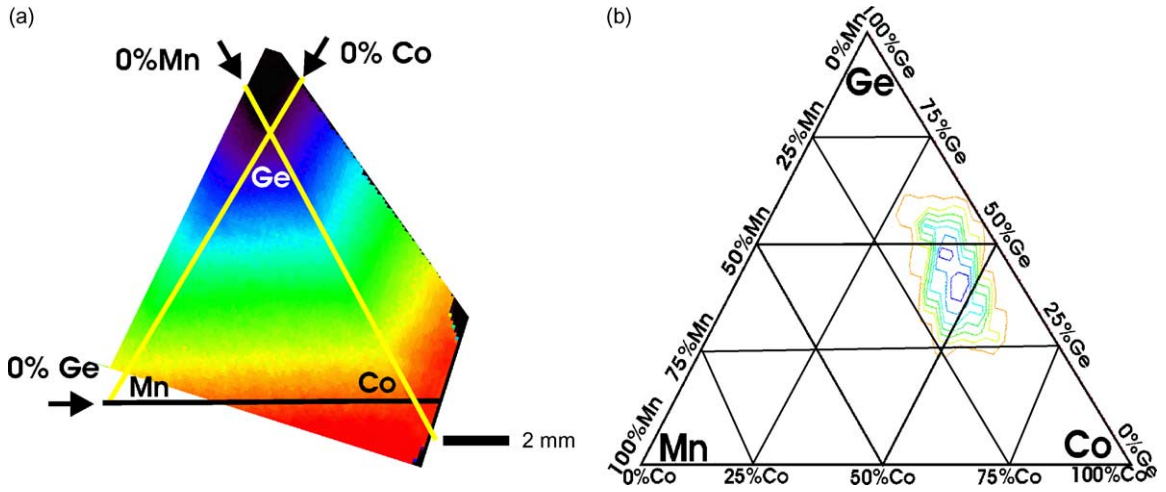

Fig. 4. (a) Image of the combined Mn and Co concentration. The 0% Mn and Co boundaries are shown in yellow. Determination of the 0% Ge boundary, shown in black, is described in the text. (b) X-ray diffraction intensity contours of a strongly ordered FCC crystalline phase shown in the ternary composition coordinates determined by the quantitative XRF analysis.

the accumulative correction factors in order to obtain the *atomic density* ratio between Mn and Co. Quantification of the absolute elemental area density, which is not called for in characterizing most combinatorial thin-films, can be achieved using standard XRF references. Because our sample was thin (∼600 Å), we ignored self-absorption effects (re-absorption of the emitted fluorescence X-ray by the film), which become important for thicker films (>1 μm). It is also important to point out that the XRF measurement probes the total number of atoms in the film, regardless of their chemical state. Consequently, microscopic phase separation, which does not alter the total number of atoms in the probed region, cannot be measured by this technique.

We visualize the combined Mn and Co concentration on the substrate obtained from the sum of the corrected Mn and Co Kα intensities in Fig. 4a. In this particular representation, the gradient direction of the combined surface concentration of Mn and Co is clearly shown, indicating the excellent calibration in the deposition rate of both Mn and Co. In addition, the composition boundaries between the binary and the ternary (i.e. along the two yellow lines) are also naturally visualized. In the absence of a direct measurement, we infer the distribution of the Ge concentration in the sample. Because of the combinatorial growth method implementing the sequential growth of the wedge profiles via 120° sample rotations, the Ge composition gradient direction is 60° away from the composition boundaries for 0% Mn and Co (yellow lines in Fig. 4a) and the position of the 100% Ge apex coincides with the interception of the two boundaries. However, the exact location of the 0% Ge boundary remains uncertain. The 0% Ge composition boundary (black line) in Fig. 4a was determined by the alignment of the shadow mask to the fiduciary marks on the sample during the sample growth, and was confirmed by comparing the diffraction measurements carried out on this ternary sample and a binary composition-spread sample $(Co_xMn_{1-x})_{0.75}Ge_{0.25}$ [10].

Having identified the 0% Ge boundary, we derived the coordinate transformation from sample position (X, Y), to ternary composition, so the crystalline phases determined from parallel XRD measurements could be mapped into the correct composition coordinates. As an example, we present, in Fig. 4b, the diffraction intensity contours of the strongly ordered FCC crystalline phase in the CoMnGe ternary alloys system.

4. Summary

We have described a synchrotron-based experimental approach for a scanning X-ray microprobe. This microprobe was used for integrating X-ray characterization of both elemental composition and crystalline structure of a ternary composition-spread, $Co_xMn_yGe_{1-x-y}$, thin-film sample. The XRF measure-

ments revealed that the Co and Mn composition distribution over the entire sample to be highly linear. Using quantitative analysis, we deduced the ternary composition as a function of the sample coordinate, from which a ternary structural phase diagram was determined.

Acknowledgements

Use of the Advanced Photon Source was supported by the U.S. Department of Energy, Office of Science Basic Energy Sciences, under Contract No. W-31-109-ENG-38. The combinatorial research at University of North Carolina is supported in part by NSF DMR-0108605. We thank Dr. Eric M. Dufresne and Jesse Guzman of the University of Michigan for experimental assistance.

References

[1] E.J. Amis, X.-D. Xiang, J.-C. Zhao, MRS Bull. 27 (4) (2002) 295–297, and the other articles in this issue.

[2] X.-D. Xiang, Appl. Surf. Sci. 189 (2002) 188–195, and references therein.

[3] F. Tsui, L. He, L. Ma, Combinatorial and artificial intelligence methods of materials science, Part I, in: Takeuchi et al. (Ed.), MRS Symposium Proceedings, vol. 700, MRS, Pittsburgh, PA, 2001, S2.2.1-6;
Y.K. Yoo, F. Tsui, MRS Bull. 27 (4) (2002) 316–323.

[4] R. Jenkins, R.W. Gould, D. Gedcke, Quantitative X-ray Spectrometry, Marcel Dekker, New York, NY, 1995.

[5] C.J. Sparks Jr., in: H. Winick, S. Doniach (Eds.), Synchrotron Radiation Research, Plenum Press, New York, 1980, pp. 459–512.

[6] Z. Cai, B. Lai, W. Yun, P. Ilinski, D. Legnini, J. Maser, W. Rodrigues, X-ray microscopy, in: T. Warwick, D. Attwood (Eds.), Proceedings of the Sixth International Conference, Meyer-Ilse, 2000, pp. 472–477.

[7] P.J. Eng, M. Newville, M.L. Rivers, S.R. Sutton, SPIE Proc. 3449 (1998) 145.

[8] P. Ilinski, B. Lai, Z. Cai, W. Yun, D. Legnini, T. Talarico, M. Cholewa, L.K. Webster, G.B. Deacon, S. Rainone, D.R. Phillips, A.P.J. Stampfl, Cancer Res. 63 (2003) 1776–1779.

[9] J.S. Iwanczyk, B.E. Patt, J. Segal, J. Plumnner, G. Vikelis, B. Hedman, K.O. Hodgson, A.D. Cox, L. Rehn, J. Metz, Nucl. Instrum. Methods A 380 (1996) 288–294.

[10] Y.S. Chu, A. Tkachuk, S. Vogt, P. Ilinski, D.A. Walko, D.C. Mancini, Eric M. Dufresne, L. He, F. Tsui, Appl. Surf. Sci., submitted for publication.